PCCP

Accepted Manuscript

ROYAL SOCIETY OF CHEMISTRY

www.rsc.org/pccp

Cite this: DOI: 10.1039/c0xx00000x

www.rsc.org/xxxxxx

ARTICLE TYPE

Controllable synthesis, morphology evolution and electrochemical properties of $LiFePO_4$ cathode materials for Li-ion batteries

Jianjun Song[a,b], Lin Wang[a], Guangjie Shao[a,b,], Meiwu Shi[c], Zhipeng Ma[a,b], Guiling Wang[a,b], Wei Song[a,b], Shuang Liu[a,b] and Caixia Wang[a,b]*

Received (in XXX, XXX) Xth XXXXXXXXX 20XX, Accepted Xth XXXXXXXXX 20XX
DOI: 10.1039/b000000x

Monodispersed $LiFePO_4$ nanocrystals with diverse morphologies were successfully synthesized via a mild and controllable solvothermal approach with a mixture of ethylene glycol and oleic acid as solvent. Morphology evolution of $LiFePO_4$ nanoparticles from nanoplates to nanorods can be simply realized by varying the volume ratio of oleic acid to ethylene glycol. Moreover, the mechanism of competitive adsorption between ethylene glycol and oleic acid was proposed for the formation of different morphologies. Electrochemical measurements show that the $LiFePO_4$/C nanorods have the initial discharge capacity of 155 mAh g^{-1} at 0.5 C with the capacity retention of 80% at a high rate of 5C, which confirms that $LiFePO_4$/C nanorods exhibit excellent rate capability and cycling stability.

1. Introduction

As a cathode material for Li-ion batteries, Olivine-type lithium iron phosphate ($LiFePO_4$) proposed by Padhi *et al.*[1] has attracted increasing attention because of its low cost, environmental compatibility, superior capacity retention, thermal stability and safety.[1-3] The main obstacles for applicable electrochemical performances are its low electronic conductivity and lithium ion diffusivity[4]. Progressive efforts, including coating $LiFePO_4$ particles with electrically conductive materials,[5-8] doping with metal ion,[9-11] minimizing the particle size[12, 13] and controlling morphology,[14-17] have been made to tackle the problems.

Considering that the electrochemical properties can be notably influenced by morphology, the synthesis of $LiFePO_4$ with various morphologies and structure is gaining expansive research interests. Wang *et al.*[18] succeeded in synthesizing $LiFePO_4$ nanowires by surfactant assisted hydrothermal method. Later, Cheng *et al.*[19] reported a novel $LiFePO_4$/C composite with sphere morphology by using 3D coralloid nitrogen-containing carbon as interpenetrating conductive framework. Most recently, the synthesis of a novel hierarchical nano/microstructure of $LiFePO_4$ microspheres consisting of nanofibers was reported by Jiang and his co-workers through a solvothermal approach with a mixture of water and 1, 2-propanediol as solvent.[20] Such $LiFePO_4$ microspheres delivered a high discharge capacity of 163.9 mAh g^{-1} at 0.1 C. However, researches on the evolution of the morphology and structure have been still rarely reported. Moreover, the controllable synthesis and the formation mechanism of $LiFePO_4$ with varieties of morphologies remain challenges in a general platform to date.

In this work, we report a morphology controllable solvothermal approach for the fabrication of $LiFePO_4$ with various well-defined morphologies by using ethylene glycol and oleic acid to regulate the nucleation and growth behaviour of the crystals. The morphology evolution from nanoplates to nanorods can be realized by simply varying the volume ratio of oleic acid to ethylene glycol. Most importantly, the formation mechanism of as-prepared nanoplates and nanorods was discussed in detail. The relation between the morphology and the electrochemical properties was also investigated.

2. Experimental Section

2.1 Preparation of materials

The nanosized $LiFePO_4$ samples were prepared using $FeSO_4{\cdot}7H_2O$, H_3PO_4 and $LiOH{\cdot}H_2O$ in a molar ratio of 1: 1: 3 by a facile solvothermal method. First, the starting materials were dissolved in ethylene glycol (EG) and then mixed with different volume of oleic acid (OA). Then, 0.015 mol of H_3PO_4 was slowly added to 25 ml of LiOH (0.045mol) solution. When a white suspension formed, 25 ml of $FeSO_4$ (0.015mol) solution was slowly introduced into the suspension under stirring for 30min. The precursor was transferred into a Teflon-lined autoclave and heated to 180 ^oC for 18 h and then cooled down to room temperature. The obtained precipitate was washed with deionized water and ethanol several times, and then dried in vacuum at 60 ^oC for 12 h.

The carbon-coated lithium iron phosphate was achieved through the esterification reaction between citric acid and ethylene glycol. The precursor and proper ethylene glycol were

added to 10 ml citric acid (5 wt%) solution under stirring, and then the solution was evaporated to yield a dark blue gel at 80 °C in water bath. Finally, the gel was carbonized for 6 h at 700 °C in nitrogen atmosphere. Different volume ratios (r= 0, 0.5, and 1) of OA to EG was applied to investigate the influence of the co-solvent on the morphology of $LiFePO_4$. For convenience, three sample notations are used in this paper: LFP $_{r=0}$, LFP $_{r=0.5}$ and LFP $_{r=1}$, respectively.

2.2 Structural Characterization

The structure of the as-prepared samples was characterized by X-ray diffraction (XRD) on a Rigaku D/max-2500/pc. The morphology and microstructure of the powder were examined with the Hitachi Model S-4800 field-emission scanning electron microscope (FE-SEM) and high-resolution transmission electron microscope (HRTEM) with model JEM2010.

2.3 Electrochemical measurements

The electrochemical performances of the samples were measured in simulative cells, which consisted of a working electrode and a lithium foil electrode separated by a Celgard 2400 microporous membrane. The working electrode was prepared by dispersing 80 wt% active materials, 10 wt% acetylene black and 10 wt% polyvinylidene fluoride (PVDF) binder in N-methyl pyrrolidone (NMP) solvent to form uniform slurry. The slurry was spread onto aluminum foil and dried in vacuum at 120 ℃ for 12 h. The electrolyte was 1 M $LiPF_6$/EC+DEC (1:1, v/v).

The cells were tested by galvanostatic charge-discharge cycling between 2.4 V and 4.2 V (versus Li/Li^+) on a battery testing system (CT2001A, LAND, China) at different current rates at room temperature. Electrochemical impedance spectroscopy (EIS) measurements were performed in an alternating current frequency range from 1 mHz to 1 MHz using a CHI660E electrochemical workstation (Chenhua, Shanghai China).

3. Results and discussions

3.1 Structural and Morphology Analysis

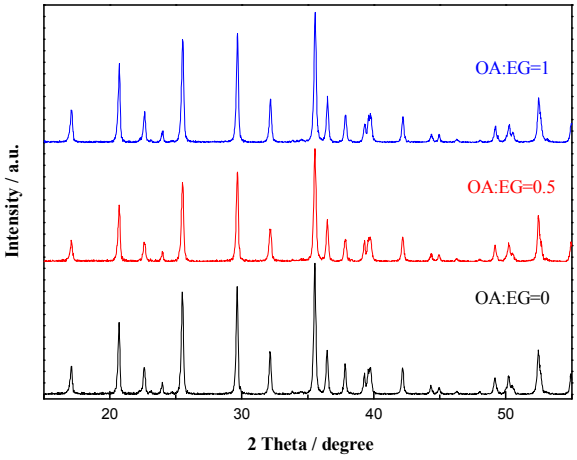

Fig. 1 XRD patterns of $LiFePO_4$/C with different volume ratios of OA/EG

The XRD patterns of $LiFePO_4$/C samples with different volume ratios of OA/EG (r= 0, 0.5, and 1) are shown in Fig. 1. Table 1 shows the corresponding structural parameters of the samples. The crystal phases of all the samples are in accordance with the ordered olivine structure indexed orthorhombic Pnma (JCPDS Card No. 83-2092), and no extra reflection peak from impurity is observed, indicating that the oleic acid has an inconspicuous effect on the purity and crystallinity of the $LiFePO_4$ phase.

Table 1 Lattice parameters of the samples

Samples	a(Å)	b(Å)	c(Å)	d of (101) facet (Å)
LFP/C $_{r=0}$	10.3482	6.0193	4.6997	4.2791
LFP/C $_{r=0.5}$	10.3403	6.0175	4.7055	4.2829
LFP/C $_{r=1}$	10.3411	6.0152	4.7155	4.2905

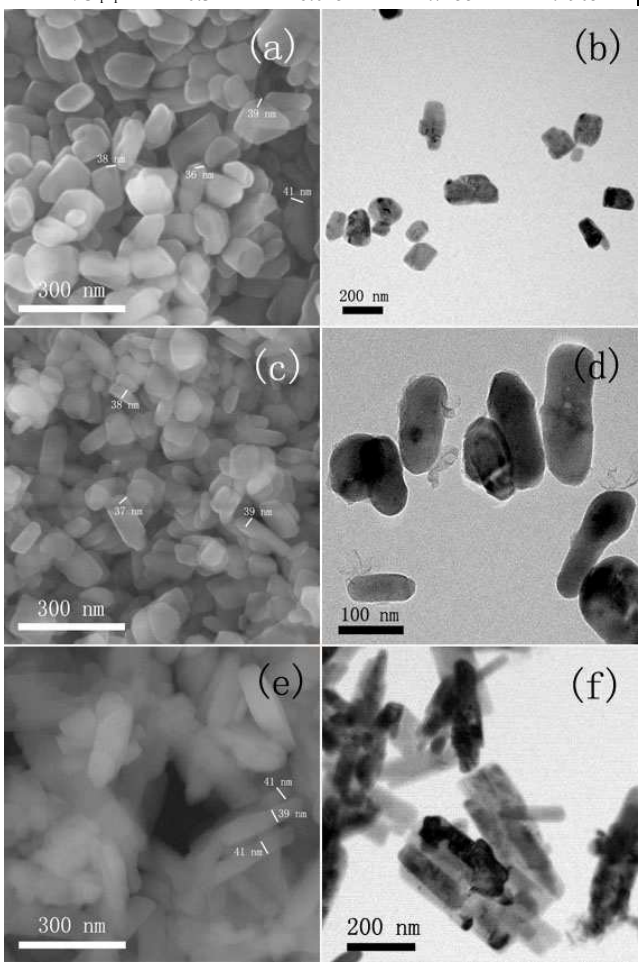

Fig. 2 FESEM images of LFP $_{r=0}$ (a), LFP $_{r=0.5}$ (c), and LFP $_{r=1}$ (e); TEM images of LFP $_{r=0}$ (b), LFP $_{r=0.5}$ (d), and LFP $_{r=1}$ (f).

Fig. 2 depicts the FESEM and TEM images of $LiFePO_4$ samples with different volume ratios of OA/EG (r= 0, 0.5, and 1). It is interesting that the morphology and particle size of $LiFePO_4$ nanocrystals could be readily controlled by tuning the ratio of OA to EG in the precursor solution. The SEM (Fig. 2(a)) and TEM (Fig. 2(b)) images show that the as-prepared $LiFePO_4$ by the solvothemal synthesis was composed of uniform nanoplates when the volume ratio of OA/EG was kept at 0, and the nanoplates have a length in the range of 100-150 nm and a width of about 100 nm. Increasing the volume ratio to 0.5 resulted in a size augment of $LiFePO_4$ nanoplates with a larger length and a repressed width, as is revealed by the Fig. 2(c) and Fig. 2(d)

images. When the volume ratio reached to 1, nanorods with a 250 nm length and a 40 nm width were obtained. It is worth noting that the three $LiFePO_4$ samples show quite similar thicknesses despite that the morphology and particle size of $LiFePO_4$ nanocrystals changed. As labeled in Fig. 2(a), (c) and (e), all the average thicknesses of three $LiFePO_4$ samples are around 40 nm. The short length along b-axis can minish the distance of Li^+ ion diffusion along the [010] direction, which are favorable for fast Li^+ ion insertion/extraction. That is, the morphology evolution from nanoplates to nanorods, rather than imposing undesirable influence, preserves the benign lithium ion diffusivity.

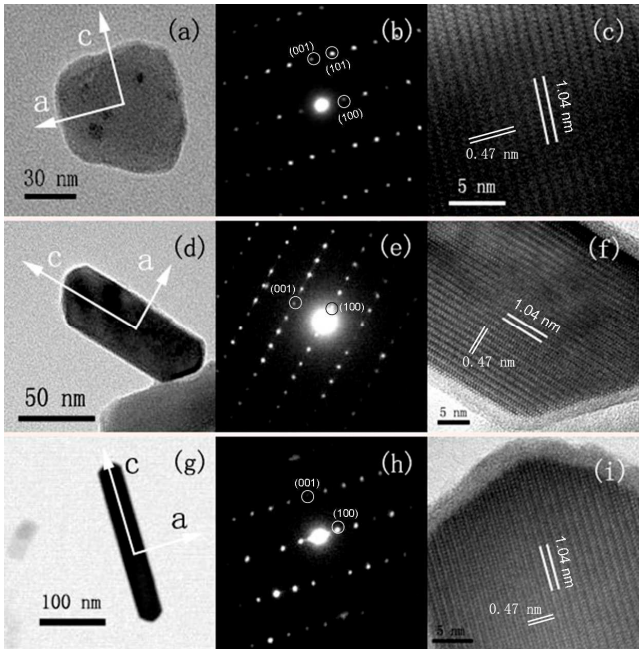

Fig. 3 Low-magnification TEM images, selected area electron diffraction (SAED) and high resolution TEM (HRTEM) images of an individual LFP $_{r=0}$ (a–c), LFP $_{r=0.5}$ (d–f) and LFP $_{r=1}$ (g–i).

Further insight into the morphology and crystal orientations of the nanosized $LiFePO_4$ samples has been gained by selected area electron diffraction (SAED) and high-resolution TEM (HRTEM). The SAED images (Fig. 3(c), (f) and (i)) of the three $LiFePO_4$ samples display well defined diffraction spots, suggesting a highly ordered single crystalline nature of the particles. The interplanar spacings of 0.47 and 1.04 nm in the HRTEM images of the as-synthesized products corresponding to (001) and (100) planes of $LiFePO_4$ further verify good crystalline state of the samples, and perfect lattice fringes distributed within the entire particle are discernible. The SAED patterns and HRTEM images indicate that crystal growth orientations along the ac plane are prominent for all the three $LiFePO_4$ samples. Besides, the $LiFePO_4$ samples grow preferentially along the [001] direction of (101) lattice planes, especially in the presence of OA.

3.2 Proposed formation mechanism

Following the evidence shown above, we suggest that the formation mechanism of different morphologies might be the competitive adsorption effect between OA and EG. When the EG was used as a soft template, nanoparticles can be transferred to nanoplates due to the effect of hydrogen bonds on the growth of the (010) plane, according to previous reports.[17, 21] The distinction among lattice planes of a $LiFePO_4$ unitcell in Fig. 4 indicates that two adjacent oxygen atoms exposed on the (010) plane might form hydrogen bonds with hydrogen atoms of EG. Additionally, the numbers of exposed oxygen atoms near the (100) and (001) planes of $LiFePO_4$ crystal are 1 and 0, respectively. Hence, EG is prone to be adsorbed on the (100) plane in comparison with (001) plane. As we know, the adsorption can lower the energy of adsorbed surface, and the crystal growth is mainly controlled by the nuclei surface energy. The fastest crystal growth will occur in the direction perpendicular to the face with the highest surface energy. Hence, there is a great possibility that the surface energy of the (010) facet was dramatically decreased by EG solvent through double-sites binding adsorption, resulting in a suppressed growth in the [010] direction, and (010) planes are more exposed in this area. In addition, the nanoplates grow preferentially along the [001] direction of the (010) plane for its higher surface energy of the (001) plane than that of (100) plane, as is observed in Fig. 2(a).

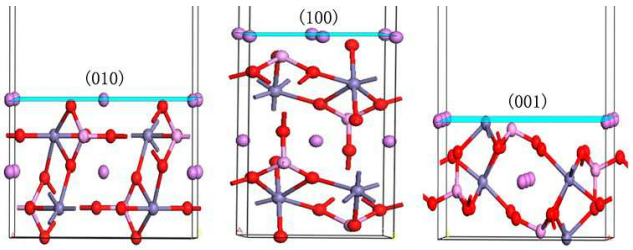

Fig. 4 The different crystal faces of a $LiFePO_4$ unitcell

When the volume ratio of OA/EG was kept at 0.5, the addition of OA had a marked influence on the morphologies of $LiFePO_4$. As an important organic surfactant, OA can be employed as a stabilizing agent and a structure-directing agent in the controlled preparation of crystal structures. OA molecules with long chains can also be adsorbed to the growing surface of nanoparticles, and lower the surface energy by forming hydrogen bonds with the oxygen atoms in $LiFePO_4$ crystal. Considering that the carbonyl of OA is an electron-withdrawing group, the OA molecules have a stronger bonding ability than EG molecules when forming hydrogen bonds with the oxygen atoms. OA exhibits the stronger capping ability on the surface of $LiFePO_4$ than EG. However, the double active groups of EG seem to have more competitive effect than OA when binding adsorption on (010) plane with the double active sites. Moreover, the alkyl group of OA molecules with long chains will hinder its adsorption with the double active sites of (010) plane because of the larger steric hinderance. Therefore, the facet (100) of the crystal has a preferential absorption of OA molecules to lower much more surface energies of the facet in virtue of its stronger hydrogen bonds than EG, and EG might still adsorb onto the (010) plane. As a result, the aspect ratio of the resultant nanoplates increases due to the reduced growth rate in the [100] direction than [001] direction, as is shown in Fig. 2(c).

When the volume ratio of OA to EG reached to 1, abundant OA molecules are adsorbed on the (100) plane, resulting in the considerable decrease of the surface energy for the (100) facet. Finally, the competitive adsorption effect between OA and EG led to the slower growth in the [100] direction and [010] direction

and prompted the formation of uniform $LiFePO_4$ nanorods. It is worth noting that the ratios of corresponding lattice parameters c/a of three samples show a slightly increase gradually, which exhibit a good correlation with the morphology analysis. The whole morphology evolution with different volume ratios of OA to EG is depicted in Fig. 5. It is just an initiatory supposal based on the basic theory of chemistry, and the detail mechanism still needs further research.

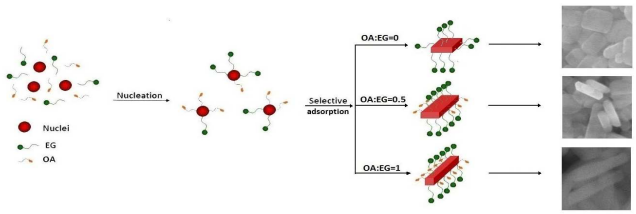

Fig. 5 Proposed morphology evolution mechanism with different volume ratios of OA/EG

3.3 Electrochemical Characterization

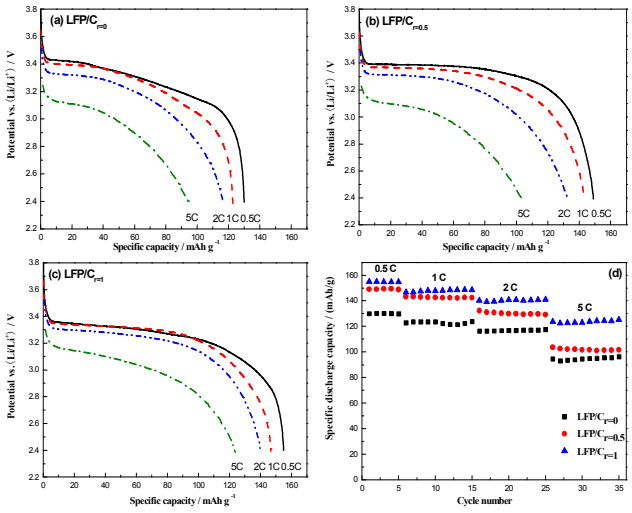

Fig. 6 Discharge curves of $LiFePO_4$/C samples with different volume ratios of OA/EG (a) r= 0, (b) r= 0.5, and (c) r= 1. (d) The cycle performance of $LiFePO_4$/C samples at different current rates

In order to evaluate systematically electrochemical performances of the three $LiFePO_4$/C samples with different volume ratios of OA/EG (r= 0, 0.5, and 1), the cells were charged and discharged at different rates from 0.5 to 5 C stepwise. The initial discharge curves of $LiFePO_4$/C samples and the corresponding cycling performance at various rates are shown in Fig. 6, in which the plateau around 3.4 V agrees well with the two-phase ($LiFePO_4$ – $FePO_4$) transformation process.[22] It can be clearly seen that $LiFePO_4$/C nanorods reveal the best rate capability among all the samples, with the discharge capacities of 155, 146.8 and 123.7 mAh g^{-1} at 0.5 C, 1 C, 2 C, and 5 C, respectively. The decreases of discharge capacity for $LiFePO_4$/C nanorods are less than those of other samples when the discharging current increases from 0.5 C to 5 C. This excellent rate capability is mainly attributed to the reduced pathway for Li ion migration and electron transportation for the unique morphology and small particle size of $LiFePO_4$/C nanorods. Previous studies[23,24] have reported that $LiFePO_4$/C nanorods can maintain an admirable electrochemical performance as a useful cathode material for lithium-ion battery. The synthesized nanorods in our study show a great decrease in the diameter compared with the aforementioned reports, and thus the electrochemical properties are remarkably enhanced.

The electrochemical impedance spectra (EIS) are used to further analyze the effect of different morphologies on the electrochemical response of $LiFePO_4$/C cathode materials. Before EIS tests, the cells are cycled for two cycles at 0.1 C rate. The electrodes were conducted at 50 % of discharge or charge state to avoid the huge potential change brought by small current alternation during EIS measurements. Fig. 7(a) shows the impedance spectra of $LiFePO_4$/C with different volume ratios of OA/EG (r= 0, 0.5, and 1). Usually, an intercept in the high frequency region of the Z′ real axis corresponds to the ohmic resistance (R_s), which represents the resistance of the electrolyte and electrode material. The semicircle in the middle frequency range indicates the double layer capacity and charge transfer resistance (R_{ct}) at electrodes. The constant phase element (*CPE*) represented for the double layer capacitance was used. The inclined line in the low frequency represents the Warburg impedance (Z_w), which is associated with lithium-ion diffusion in the $LiFePO_4$ particles. The parameters in the equivalent circuit are calculated and tabulated in Table 2. The $LiFePO_4$/C nanorods exhibit a smaller R_{ct} than the other two samples, which is convenient for rapid electrochemical reaction.

The exchange current density (I_0) is a very important parameter of kinetics for an electrochemical reaction, and can measure the catalytic activity of electrodes. It is calculated using the following formula:

$$I_0 = \frac{R \cdot T}{nR_{ct} \cdot F} \qquad (1)$$

Where R is the gas constant (8.314 J mol^{-1} K^{-1}), T is the temperature (298 K), n is the charge transfer number per molecule during the intercalation, and F is the Faraday's constant (96,500 C mol^{-1}). The highest I_0 of $LiFePO_4$/C nanorods shown in table 2 implies the best catalytic activity and reversibility among the three $LiFePO_4$/C samples, which is in prefect agreement with its excellent electrochemical performance.

The lithium ion diffusion coefficients (D) of $LiFePO_4$/C with different volume ratios of OA/EG (r= 0, 0.5, and 1) are also calculated according to the following equation:

$$D = \frac{R^2T^2}{2A^2n^4F^4C^2\sigma^2} \qquad (2)$$

where R is the gas constant, T is the absolute temperature, A is the surface area of the cathode, n is the number of electrons per molecule during oxidization, F is the Faraday constant, C is the concentration of lithium ion, and σ is the Warburg factor which has relationship with Z' :

$$Z' = R_D + R_C + \sigma\omega^{-\frac{1}{2}} \qquad (3)$$

Fig. 7(b) shows the relationship between Z' and square root of frequency ($\omega^{-1/2}$) in the low-frequency region. The diffusion

coefficient of lithium ion is calculated based on Eqs. 2 and 3. The calculated lithium ion diffusion coefficients of $LiFePO_4$/C with different volume ratios of OA/EG (r= 0, 0.5, and 1) are 1.09×10^{-14}, 3.08×10^{-14} and 1.37×10^{-12} cm^2 s^{-1}, respectively. The result might be owing to the transition from 2D to 1D system. Importantly, the small size along a axis of nanorod can induce the lattice relaxation, further possessing a enlarged interplanar distance of (101) crystal plane, which can be proved in Table 1. This means a wider Li ion diffusion pathway in [010] direction. Therefore, the $LiFePO_4$/C nanorods show the highest lithium ion diffusion coefficients, which is consistent with the Bi's report.[25]

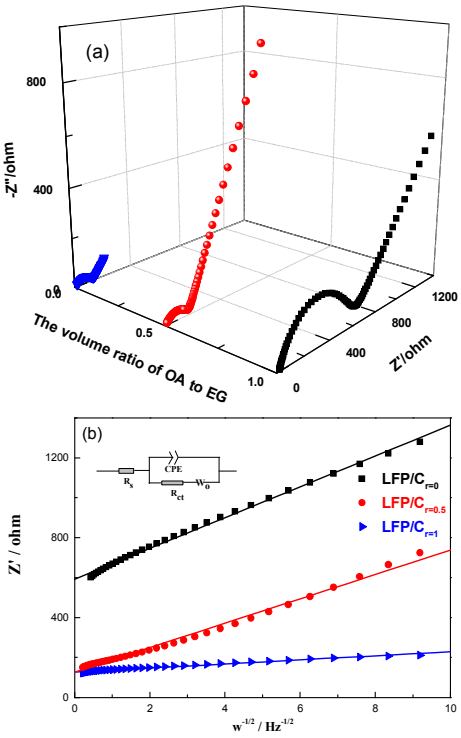

Fig. 7 (a) The EIS spectra of $LiFePO_4$/C with different volume ratios of OA/EG (r= 0, 0.5, and 1). (b) The equivalent circuit used for fitting the experimental EIS data (inset) and the relationship between Z' and square root of frequency ($\omega^{-1/2}$) in the low-frequency region

Table 2 Results of electrochemical impedance and exchange current density

Samples	R_s (Ω)	R_{ct} (Ω)	I_0 (mAh·g^{-1})
LFP/C $_{r=0}$	17.09	564.3	22.8
LFP/C $_{r=0.5}$	3.268	163.4	78.5
LFP/C $_{r=1}$	9.876	120.6	107.0

The EIS results make it clear that the increase of the exchange current density and the lithium ion diffusion coefficient resulted from the unique morphology and small particle size of nanorods leads to the elevated electrochemical activity of $LiFePO_4$/C.

4. Conclusion

$LiFePO_4$ nanocrystals with different morphologies were successfully synthesized by a facile solvothermal approach with a mixture of ethylene glycol and oleic acid as solvent. It can be identified that the presence of OA plays an important role in controlling the morphology evolution and the particle size of $LiFePO_4$ crystal, which might be attributed to the competitive adsorption between ethylene glycol and oleic acid. The $LiFePO_4$/C nanorods exhibit the best electrochemical performance among the three samples, with the initial discharge capacity of 155 mAh g^{-1} at 0.5 C, even 123.7 mAh g^{-1} at a high rate of 5 C. In summary, the controllable synthesis of different morphologies is an effective way to improve the performance of $LiFePO_4$ as cathode material for rechargeable lithium ion batteries.

Acknowledgment

We are grateful for the financial support from the Natural Science Research Keystone Program of Universities in Hebei Province China (No. ZH2011228) and the Natural Science Foundation in Hebei Province China (No. B2012203069).

Notes and References

[a] Hebei Key Laboratory of Applied Chemistry, College of Environmental and Chemical Engineering, Yanshan University, Qinhuangdao 066004, China
[b] State key Laboratory of Metastable Materials Science and Technology, Yanshan University, Qinhuangdao 066004, China
[c] The Equipment Research Institute of the General Logistic Department of the Chinese People's Liberation Army, Beijing 100010, China
Tel & fax: 0086-335-8061569. E-mail address: shaoguangjie@ysu.edu.cn

[1] A.K. Padhi, K.S. Nanjundaswamy and J.B. Goodenough, *J. Electrochem. Soc.*, 1997, **144**, 1188-1194.
[2] J. Wang and X. Sun, *Energy Environ. Sci.*, 2012, **5**, 5163-5185.
[3] S. Nishimura, G. Kobayashi, K. Ohoyama, R. Kanno, M. Yashima and A. Yamada, *Nat. mater.*, 2008, **7**, 707-711.
[4] L.X. Yuan, Z.H. Wang, W.X. Zhang, X.L. Hu, J.T. Chen, Y.H. Huang and J.B. Goodenough, *Energy Environ. Sci.*, 2011, **4**, 269-284.
[5] C.R. Sides, F. Croce, V.Y. Young, C.R. Martin and B. Scrosati, *Electrochem. Solid-State. Lett.*, 2005, **8**, A484- A487.
[6] Y.S. Hu, Y.G. Guo, R. Dominko, M. Gaberscek, J. Jamnik and J. Maier, *Adv. Mater.*, 2007, **19**, 1963-1966.
[7] C.H. Mi, Y.X. Cao, X.G. Zhang, X.B. Zhao and H.L. Li, *Powder. Technol.*, 2008, **181**, 301-306.
[8] K.S. Park, J.T. Son, H.T. Chung, S.J. Kim, C.H. Lee, K.T. Kang and H.G. Kim, *Solid State Commun.*, 2004, **129**, 311-314.
[9] I. Bilecka, A. Hintennach, M.D. Rossell, D. Xie, P. Novak and M. Niederberger, *J. Mater. Chem.*, 2011, **21**, 5881-5890.
[10] Z.L. Wang, S.R. Sun and D.G. Xia, *J. Phys. Chem. C*, 2008, *112*, 17450-17455.
[11] Y. Ge, X. Yan, J. Liu, X. Zhang, J. Wang, X. He, R. Wang and H. Xie, *Electrochim. Acta*, 2010, **55**, 5886-5890.
[12] D. Choi and P.N. Kumta, *J. Power Sources*, 2007, **163**, 1064-1069.
[13] C. Delacourt, P. Poizot, S. Levasseur and C. Masquelier, *Electrochem. Solid-State. Lett.*, 2006, **9**, A352-A355.
[14] N. Zhou, H. Wang, E. Uchaker, M. Zhang, S. Liu, Y. Liu and G. Cao, *J. Power Sources*, 2013, **239**, 103-110.
[15] Z. Huang, S. Oh, Y. He, B. Zhang, Y. Yang, Y. Mai and J. Kim, *J. Mater. Chem.*, 2012, **22**, 19643-19645.
[16] N. Zhou, E. Uchaker, H. Wang, M. Zhang, S. Liu, Y. Liu, X. Wu, G. Cao and H. Li, *RSC Advances*, 2013, **3**, 19366-19374.
[17] D. Rangappa, K. Sone, T. Kudo and I. Honma, *J. Power Sources*, 2010, **195**, 6167-6171.
[18] G. Wang, X. Shen, and J. Yao, *J. Power Sources*, 2009, **189**, 543-546.
[19] F. Cheng, S. Wang, A. Lu and J. Yao, *J. Power Sources*, 2013, **229**, 249-257.
[20] Y. Jiang, S. Liao, Z. Liu, G. Xiao, Q. Liu and H. Song, *J. Mater. Chem. A*, 2013, **1**, 4546-4551.
[21] K. Saravanan, M. V. Reddy, P. Balaya, H. Gong, B. V. R. Chowdari and J. J. Vittal, *J. Mater. Chem.*, 2009, **19**, 605-610.

[22] J. F. Ni, M. Morishita, Y. Kawabe, M.Watada, N. Takeichi and T. Sakai, *J. Power Sources*, 2010, **195**, 2877-2882.
[23] F. Teng, M. Chen, G. Li, Y. Teng, T. Xu, S. Mho and X. Hua, *J. Power Sources*, 2012, **202**, 384-388.
[24] X. Huang, S. Yan, H. Zhao, L. Zhang, R. Guo, C. Chang, X. Kong and H. Han, *Mater. Charact.*, 2010, **61**, 720-725.
[25] Z. Bi, X. Zhang, W. He, D. Min and W. Zhang, *RSC Adv.*, 2013, **3**, 19744-19751.

Graphical Abstract

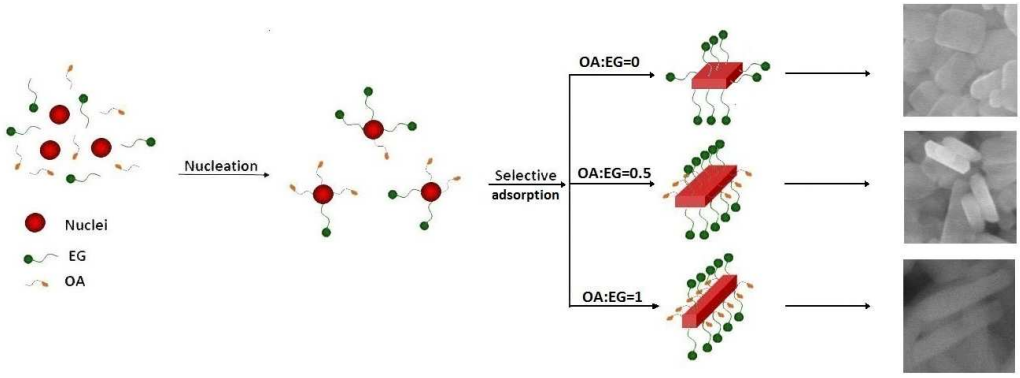

In this review, the mechanism of competitive adsorption between ethylene glycol and oleic acid was proposed for the morphology evolution of $LiFePO_4$ nanoparticles from nanoplates to nanorods.